



Photocatalytic H₂ Production from Water with Rhenium and Cobalt Complexes

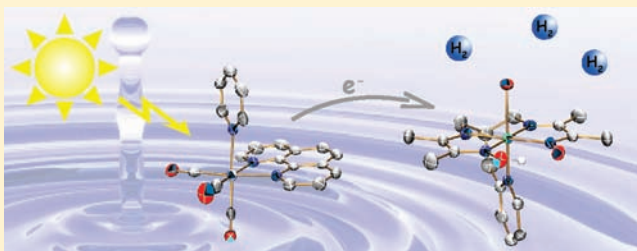
Benjamin Probst,^{†,§} Miguel Guttentag,[†] Alexander Rodenberg,[‡] Peter Hamm,^{*,†} and Roger Alberto^{*,†}

[†]Institutes of Inorganic and [‡]Physical Chemistry, University of Zürich, Winterthurerstrasse 190, CH-8057 Zürich, Switzerland

 Supporting Information

 Web-Enhanced

ABSTRACT: Photocatalytic hydrogen production in pure water for three component systems using a series of rhenium-based photosensitizers (PS) and cobalt-based water reduction catalysts (WRC), with triethanolamine (TEOA) as an irreversible electron donor, is described. Besides the feasibility of this reaction in water, key findings are reductive quenching of the excited state of the PS by TEOA ($k_q = 5-8 \times 10^7 \text{ M}^{-1} \text{ s}^{-1}$; $\Phi_{\text{cage}} = 0.75$) and subsequent transfer of an electron to the WRC ($k_{\text{Co}^{\text{III}}} = 1.1 \times 10^9 \text{ M}^{-1} \text{ s}^{-1}$). Turnover numbers in rhenium ($\text{TON}_{\text{Re}}, \text{H}/\text{Re}$) above 500 were obtained, whereas TON_{Co} (H_2/Co) did not exceed 17. It is shown that the cobalt-based WRC limits long-term performance. Long-term performance critically depends on pH and the type of WRC used but is unaffected by the type of PS or the concentration of WRC. A quantum yield of 30% was obtained (H/photon).



INTRODUCTION

Limited fossil and nuclear fuel reserves will make alternative energy resources crucial for the 21st century. Solar energy plays a key role, and all modalities to harvest and convert light must be explored in great detail.¹ Classical PV cells convert sunlight into electrical energy which can be used for water splitting. An appealing alternative is direct, photocatalytic water splitting into H₂ and O₂, mimicking photosynthesis. Conceptually, a photosensitizer (PS) harvests sunlight, and water oxidation and reduction catalysts (WOC and WRC) complete the overall reaction. The system can be split into its reductive and oxidative parts and then be studied independently. Ideally, these processes run directly in water as a solvent.

Closed cycles for photochemical water splitting in homogeneous solution with visible light are not yet available. Since the 1980s, detailed studies for the reductive half reaction have been presented with $[\text{Ru}(\text{bipy})_3]^{2+}$, $[\text{ReBr}(\text{CO})_3\text{bipy}]$, $[\text{Ir}(\text{ppy})_2(\text{bipy})]^+$, $[\text{Pt}(\text{tpy})\text{acetylide}]^+$, or xanthene as PSs.²⁻¹⁵ Common WRCs are $[\text{M}(\text{bipy})_3]^{3+}$ ($\text{M} = \text{Rh}$ or Co),²⁻⁴ cobalt macrocyclic complexes,^{5-9,15-20} or colloidal Pt/Pd in combination with electron relays (e.g. MV²⁺).^{11,21} TEOA, ascorbate, or Eu²⁺ often serve as sacrificial electron donors. These systems produced H₂ in organic or mixtures of organic solvents and H₂O. Some early kinetic and mechanistic studies by Sutin and co-workers with Ru/Co catalysts evidenced H₂ formation in homogeneous aqueous solution.^{2,21} It was shown that increasing amounts of water in organic solvents rapidly decreased the TON and TOF (turn over number and frequency) of H₂ formation.^{4,6,22} No homogeneous system with rhenium in water has been reported so far. A limited number of photocatalytic oxidative half reactions in homogeneous, pure aqueous solution were described.²³⁻²⁶

The maximal turnover number (TON) reported in a photochemical system for H₂ was 9000, using a rhodamine-based PS (TON_{PS} ; cobaloxime type WRC ($\text{TON}_{\text{WRC}} = 125$), TEOA as an electron donor, in MeCN/H₂O (1/1))¹⁵ and for O₂, 350 (TON_{WOC} ; using a $[\text{Ru}_4\text{-POM}]$ type WOC, $[\text{Ru}(\text{bipy})_3]^{2+}$ as a PS, and S₂O₈²⁻ as an electron acceptor, in H₂O).²⁵ Whereas oxidative half reactions do run in H₂O, well-defined water reducing systems have not been described so far. It stands to reason that a complete, homogeneous water splitting cycle must combine WOC and WRC and ultimately be performed in this solvent. We report herein a homogeneous Re/Co-based system for photocatalytic water reduction in pure H₂O.

RESULTS AND DISCUSSION

Eight photosensitizers, based on the *fac*-{Re(CO)₃} core (**1–8**, Scheme 1, for photophysical properties, see Table 1), and nine cobalt-based WRCs (**10–18**, Scheme 2) were investigated for photocatalytic hydrogen production in water. Irradiating 10 mL of an aqueous solution containing 30 μM **1**, **2**, **5**, or **6**; 500 μM **10**; 1 M TEOA; and 0.1 M HBF₄ produced ~16 μmol of H₂ ($\text{TON}_{\text{Re}} \approx 110$, H/Re; $\text{TON}_{\text{Co}} \approx 3$, H₂/Co), as depicted in Figure 1. No H₂ formation within our detection limits was observed in water for **4**, **7**, **8**, or $[\text{Ru}(\text{bipy})_3]^{2+}$ as PS, or if no PS, WRC or TEOA was added. It is known that excited $[\text{Ru}(\text{bipy})_3]^{2+}$ ($\tau \approx 900$ ns) does not interact with TEOA in H₂O.^{4,11} In a similar scheme using DMF as a solvent, H₂ production was reported and found to be initialized by a reductive quenching of excited $[\text{Ru}(\text{bipy})_3]^{2+}$ by TEOA.^{8,9} H₂ production for the rhenium-based PSs can be

Received: November 19, 2010

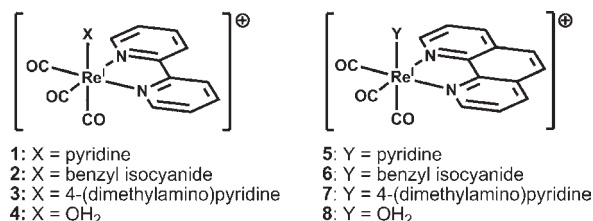
Published: March 02, 2011

Table 1. Photophysical Properties of 1–8 in H₂O

compd.	λ_{MLCT} , nm (ϵ , M ⁻¹ s ⁻¹)	λ_{phos} , nm ($\Phi \times 10^3$)	τ , ns	$E_{\text{p,a}}$ (PS ^{+2/+}), V ^b	$E_{1/2}$ (PS ⁺⁰), V ^b
1	343 (3650)	567 (10)	200	<i>c, d</i>	-1.04
2	337 (<i>sh</i> , 3800)	527 (90)	1'200	<i>c, d</i>	-1.10
3	368 (2450)	602 (0.30)	13	1.6 ^c	-1.06
4	339 (<i>sh</i> , 4000) ^a	585 (0.25) ^a	8.5 ^a	1.4 ^c	-1.09
5	362 (3350)	550 (40)	1'200	<i>c, d</i>	-1.01
6	360 (<i>sh</i> , 2600)	515 (210)	12'800	<i>c, d</i>	-1.08
7	368 (3000)	592 (1.0)	58	1.6 ^c	-1.03
8	360 (<i>sh</i> , 3400) ^a	578 (1.0) ^a	28 ^a	1.4 ^c	-1.07

^a 1 mM TfsOH, H₂O. ^b $E_{\text{p,a}}$ and $E_{1/2}$ are the anodic and half-wave peak potentials, respectively, in V vs Ag/AgCl (referenced to Fc^{0/+} at 500 mV), measured in DMF containing 0.1 M TBA[PF₆]. ^c Irreversible process. ^d > 1.6 V.

Scheme 1. Schematic Drawings of Photosensitizers 1–8



correlated with excited state lifetimes as reported in Table 1.²⁷ Reductive quenching of the excited state by TEOA occurs on a time scale of 10–100 ns ($k_{\text{q}} \approx 10^7 - 10^8 \text{ M}^{-1} \text{ s}^{-1}$; see Electron Transfer section), thus allowing for efficient quenching in the cases of 1, 2, 5, and 6, but less so for 3, 4, 7, and 8. This was confirmed by measuring the H₂ production with 3, which proceeded at very low rates but gave identical amounts of H₂ compared to that observed for 1, 2, 5, and 6.²⁸ In the case of 7, solubility issues in the buffer system used for catalysis prevented H₂ production experiments. Catalysis for the two aquo complexes 4 and 8 was found to be inhibited by deprotonation of coordinated H₂O in the ground ($\text{p}K_{\text{a}}(4, \text{H}_2\text{O}) = 8.5$) and in the excited state (see Electron Transfer section).

Time resolved vibrational spectroscopy was applied for complexes 1, 4, 5, and 8 in order to quantitatively study the initial reaction steps in the picosecond to microsecond domain (see Electron Transfer section).²⁹ Since these may be different from organic solvents, we focused on the initial set of reactions in rhenium. It is of fundamental interest to elucidate whether oxidative or reductive quenching of the excited state takes place and how fast it is (k_{q}).³⁰ It was of further interest to quantify the efficiency of the quenching process and to observe subsequent electron transfers.

Electron Transfer. In DMF, photocatalytic H₂ production is initiated by reductive quenching of the excited PS.^{9,19} To assess the mechanistic sequence in H₂O, we performed time-resolved vibrational spectroscopy in the picosecond to microsecond time range in D₂O.³¹ Upon excitation with a 400 nm laser pulse, we see within the response time of our setup instantaneous formation of the ³MLCT state *1, characterized by a blue shift in absorption (depopulation of 1 results in a bleach of $\nu_{\text{CO, sym}}$ at 2034 cm⁻¹ and overlapping $2 \times \nu_{\text{CO, asym}}$ at 1932 cm⁻¹, whereas population of *1 gives positive readings at 2070, 2016, and 1971 cm⁻¹ for $\nu_{\text{CO, sym}}$ and $2 \times \nu_{\text{CO, asym}}$),^{32–38} its lifetime being 200 ns (Figure 2, yellow trace).

In the presence of 1 M TEOA and 0.1 M HBF₄, we again see the immediate formation of *1, followed by reductive quenching

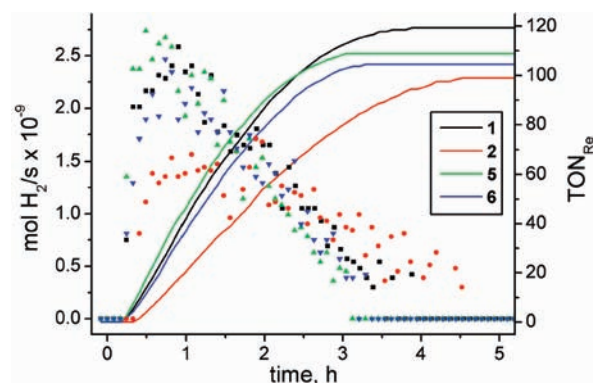


Figure 1. H₂ production with 1, 2, 5, and 6 (mol/s, left scale, dots; TON_{Re}, right scale, solid lines; 30 μM PS, 500 μM 10, 1 M TEOA, 0.1 M HBF₄, H₂O, 10 mL, 380 nm, $q_{\text{h,p}} = 1.75 \times 10^{-7} \text{ einstein/s}$).

yielding 1⁻ (characterized by a red shift of absorption, $\nu_{\text{CO, sym}}$ at 2012 and overlapping $2 \times \nu_{\text{CO, asym}}$ at 1895 cm⁻¹; Figure 2, blue trace).^{36,39} An exponential fit yielded a time constant of 20 ns, thus resulting in a bimolecular quenching rate of about $5 \times 10^7 \text{ M}^{-1} \text{ s}^{-1}$ (Table 2). The yield of reductive quenching, Φ_{red} , can be estimated by a comparison of the bleach of the ground state at the respective times directly after excitation and when quenching is completed (Table 2). An equivalent experiment was carried out for PS 5. Since 1 and 5 are relatively long-lived, only minor contributions of radiative and nonradiative deactivation did occur on the time scale of reductive quenching, giving rough estimates for the cage escape yield (Φ_{cage}) of 0.75 for both complexes (Table 2). Although 1⁻ decomposed in solution (see Long-Term Performance section), it was found to be stable on the time scale of up to 20 μs (see Figures 2 and 3, blue traces). In contrast to similar experiments in DMF, no transfer of a second electron from (HOCH₂C[•]H)N(CH₂CH₂OH)₂ and/or (HOC[•]HCH₂)N(CH₂CH₂OH)₂ could be observed on this time scale.¹⁹

To investigate possible oxidative quenching of *PS by WRC, a series of experiments with the long-lived PS 5 and varying concentration of 10 was performed in D₂O, without TEOA. No oxidative quenching could be detected, although rapid deactivation occurred ($k_{\text{q},10} = 1.3 \times 10^9 \text{ M}^{-1} \text{ s}^{-1}$), most likely by energy transfer from *5 to 10. Although this is a fast reaction, it does not decrease the performance of the system under study, since interaction of *PS with TEOA is more than an order of magnitude faster (because [TEOA] ≫ [WRC]). It is, however, noteworthy, since oxidative quenching of the excited

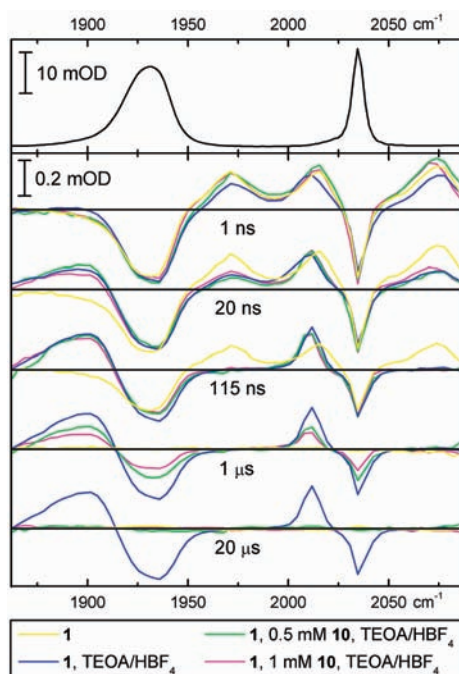


Figure 2. Top: FT-IR spectrum of the ground state of **1**, showing the characteristic $\nu_{\text{CO, sym}}$ at 2034 and overlapping $2 \times \nu_{\text{CO, asym}}$ at 1932 cm^{-1} . Below: Difference spectra after a 400 nm excitation pulse at given delays. Negative bands are due to depopulation of the ground state of **1**; positive bands are due to the population of new transient species: *1 ($\nu_{\text{CO, sym}}$ at 2070 and $2 \times \nu_{\text{CO, asym}}$ at 2016 and 1971 cm^{-1}) and 1^- ($\nu_{\text{CO, sym}}$ at 2012 and overlapping $2 \times \nu_{\text{CO, asym}}$ at 1895 cm^{-1}). Conditions: 0.25 mM **1**, varying **10**, except for yellow trace 1 M TEOA and 0.1 M HBF_4 , solvent: D_2O . An animated image of a related experiment is available in the HTML version of this manuscript as a Web Enhanced Object.

Table 2. Kinetic Parameters Obtained from Global Fitting Analysis of UV-Pump-IR-Probe Experiments with **1 and **5** as PS in D_2O**

compd.	$k_{q, \text{TEOA}}$ $\times 10^6 \text{ M}^{-1} \text{ s}^{-1}$	Φ_{red}^b	Φ_{cage}^b	$k_{\text{Co}^{\text{III}}}$ $\times 10^9 \text{ M}^{-1} \text{ s}^{-1}$
1 ^a	51	0.70	0.75	1.1
5 ^a	78	0.75	0.75	1.1

^a 0.25 mM PS, varying **[10]**, 1 M TEOA, 0.1 M HBF_4 , D_2O , solution degassed with Ar, excitation by 400 nm laser pulse; ^b $\Phi_{\text{cage}} = \Phi_{\text{red}} / \Phi_{q, \text{max}}$; $\Phi_{q, \text{max}} = (k_q[\text{Q}]) / (k_q[\text{Q}] + k_{\text{nr}} + k_t)$; Φ_{red} from the experiment.

$[\text{Pt}(\text{ttpy})(\text{acetylde})]^+$ -type PS by cobaloximes has been postulated for a similar system.⁶

To establish the rate of electron transfer from PS^- to WRC, we probed solutions containing PS, TEOA, HBF_4 , and varying concentrations of WRC. In an experiment with 250 μM **1**, 1 M TEOA, 0.1 M HBF_4 , and varying **[10]**, we again observed rapid formation of 1^- and subsequent decay of 1^- to **1**, with decay times (k_{obs}^{-1}) of $\gg 40 \mu\text{s}$, 1.92 μs , 1.90 μs , 860 and 890 ns for **[10]** = 0, 0.5, 0.5, 1, and 1 mM, respectively (see Figure 3). Since $[\text{*PS}] \approx 20 \mu\text{M}$, this allowed plotting of k_{obs} vs **[10]** according to a pseudo-first-order rate law, giving a rate constant for electron transfer from 1^- to **10** of $k_{1,10} = 1.1 \times 10^9 \text{ M}^{-1} \text{ s}^{-1}$ (see inset, Figure 3). The same value was obtained in an analogous experi-

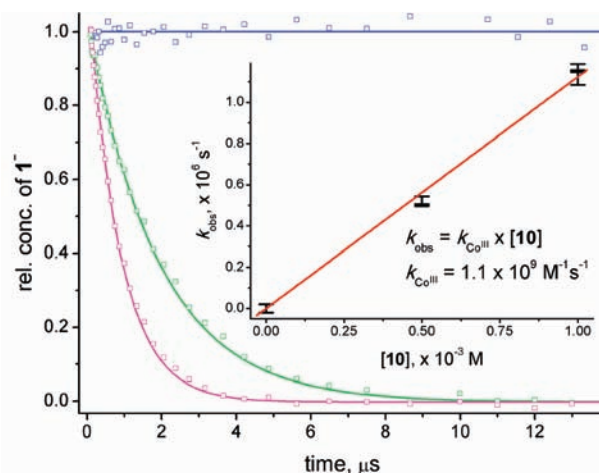


Figure 3. Relative concentration of 1^- upon 400 nm excitation at 0 (blue), 0.5 (green), and 1 (magenta) mM **10** (0.25 mM **1**, 1 M TEOA, 0.1 M HBF_4 , D_2O). Inset: Plot of k_{obs} vs **[10]** (0, 2 \times 0.5, and 2 \times 1 mM, respectively) according to a pseudo-first-order rate law. Note that the data at 0.5 mM and 1.0 mM have been measured twice, in order to verify the reproducibility of the measurement.

ment with **5**. Hence, the catalytic cycle in water follows the same sequence as in DMF: reductive quenching of *1 to 1^- with subsequent electron transfer to cobalt.^{9,19}

In addition to elucidating the reaction mechanisms for the PSs **1** and **5** above, the question was tackled why catalytic systems employing the aquo complexes **4** and **8** do not produce any hydrogen. To resolve this issue, UV-pump-IR-probe spectra were measured for **4** and **8** under identical reaction conditions as before for **1** and **5** (Figure 4). At pH 8.7, **4** is found as a mixture of its aquo ($\nu_{\text{CO, sym}}$ at 2034 and overlapping $2 \times \nu_{\text{CO, asym}}$ at 1927 cm^{-1}) and its deprotonated form, hydroxo-**4** ($\nu_{\text{CO, sym}}$ at 2016 and $2 \times \nu_{\text{CO, asym}}$ at 1909 and 1892 cm^{-1} , respectively). After excitation at 400 nm, the excited state of hydroxo-**4** decays with a time constant of ~ 0.5 ns, therefore being too short-lived for efficient reductive quenching. In contrast, *4 itself is longer lived and reacts as a photoacid, i.e., loses a proton (~ 5 ns), yielding positive absorptions at 1892, 1909, and 2016 cm^{-1} , which correspond to the ground state absorption of hydroxo-**4**, as shown in Figure 4. Afterward, equilibrium is restored with a time constant of ~ 70 ns, which is beyond the diffusion controlled ($k_{\text{d, H}_2\text{O}} \sim 10^{10} \text{ M}^{-1} \text{ s}^{-1}$) maximal possible electron transfer rate to **10**. This finding supports the assumption that *4 and *8 react as photoacids while not being reductively quenched with TEOA and therefore not initiating the catalytic cycle for hydrogen generation.

Long-Term Performance. Although good turnovers in Re were obtained ($\text{TON}_{\text{Re}} \geq 100$; H/Re), similar systems in DMF produced TON_{Re} 's up to 6000.¹⁹ Furthermore, TON_{Co} 's from **10** in water are very low (3.3; H_2/Co) compared to the 1000 turnovers as obtained in DMF.¹⁹ The first evidence concerning long-term performance came from H_2 production with different PSs: TON_{Re} 's were constant for the four PSs **1**, **2**, **5**, and **6** (see Figure 1), indicating that decomposition of **10** rather than the PS is decisive. Varying the concentration of **10** but keeping all other parameters constant, TON_{Co} 's did not change (see Figure SI 1, Supporting Information), evidencing once more the cobalt WRC being the performance limiting factor. The addition of an excess of dmgH_2 relative to **10** increased TON_{Co} but did not change the

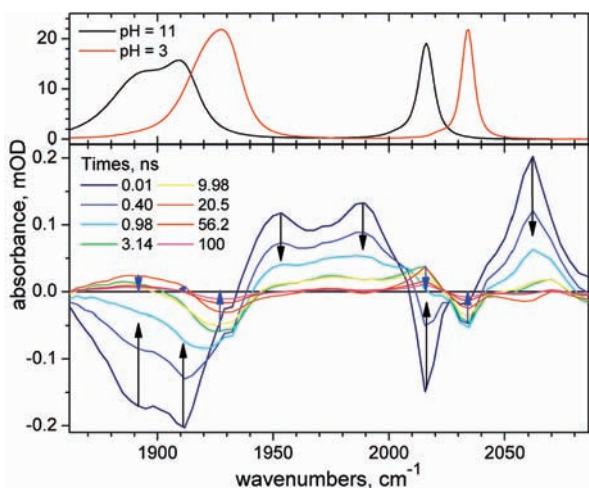


Figure 4. Top: FT-IR spectra of **4** at pH = 3 (aquo form, red line) and pH = 11 (hydroxo form, black line). Bands at 2034 and 1927 cm^{-1} belong to $\nu_{\text{CO,sym}}$ and $2 \times \nu_{\text{CO,asym}}$ of **4**, respectively, while the bands at 2016, 1909, and 1892 cm^{-1} are caused by the deprotonated form, i.e., hydroxo-**4**. Bottom: Difference absorption spectra at indicated delays after 400 nm excitation of an aqueous solution containing 0.5 mM **4**, 0.5 mM **10**, 1 M TEOA, 0.1 M HBF₄, and D₂O under Ar. Black arrows indicate the decay (~ 0.5 ns) of the excited state and bleach recovery of hydroxo-**4**, while the blue arrows point out protonation of hydroxo-**4** going along with simultaneous recovery of **4** (~ 70 ns).

rate of H₂ formation. Obviously, consumption of dmgH₂ limits the overall performance (increased TON_{Co}) while dissociation of dmgH₂ from **10** is not limiting in water (constant rate). Solutions of **10** in water are stable both in the dark and under irradiation with visible light. Only in 1 M TEOA/0.1 M HBF₄ and after several days was partial replacement of one pyridine of **10** observed. The decomposition pathway of the WRC, rationalizing the low TON_{Co}, is unknown so far. Decomposition has been observed before,^{5,19} and the reduction of coordinated dmgH to 2-aminobutan-3-one oxime was proposed,⁴⁰ rationalizing the observed [dmgH₂] dependence.

To improve the TON_{Co}, a series of WRCs (**11–18**), containing the tetradentate ligand frameworks 2,3,9,10-tetramethyl-1,4,8,11-tetrazaundecane-1,3,8,10-tetraene-1,11-diol (DOH₂) or the 2,3,9,10-tetramethyl-1,4,8,11-tetraazacyclotetradeca-1,3,8,10-tetraene (TIM), were evaluated under identical conditions to those of **10** (Scheme 2 and Figure 5). TON_{Co} > 10 was achieved for **15** (QY = 30%; H₂/photon). The ligand framework of the WRC seems to be crucial in determining the long-term stability, which increases along the series TIM < dmgH < DOH. The comparison of **11** and **15** reveals a distinct effect on catalysis imposed by the pendant pyridine moiety in **15**. Identical experiments with **11** in the presence of free pyridine did not change the performance, indicating that the higher TONs as observed for **15** compared to **11** are related to the intramolecular base.

To complement stability studies of WRCs, we studied the behavior of the PS with respect to long-term stability. Compound **1** rapidly disappeared upon irradiation in deaerated solution in the presence of TEOA but in the absence of WRC. HPLC analysis evidenced a loss of the axial pyridine ligand and formation of the solvato-complex **4**. Since reductive quenching of ***1** did take place, the product **1**⁻ underwent further reactions, ultimately resulting in the loss of the axial pyridine, as reported before.⁴¹ In the same experiment but without TEOA or in the

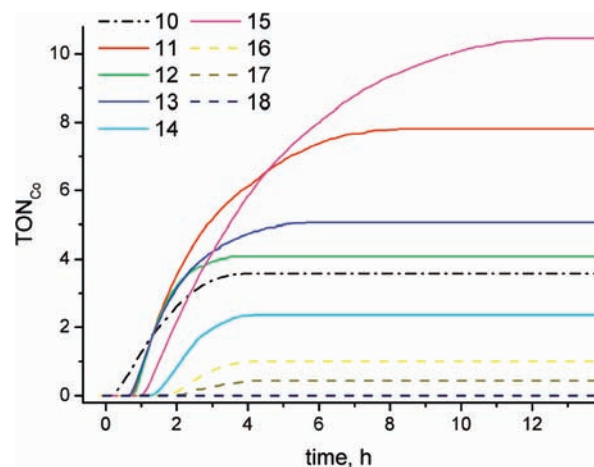
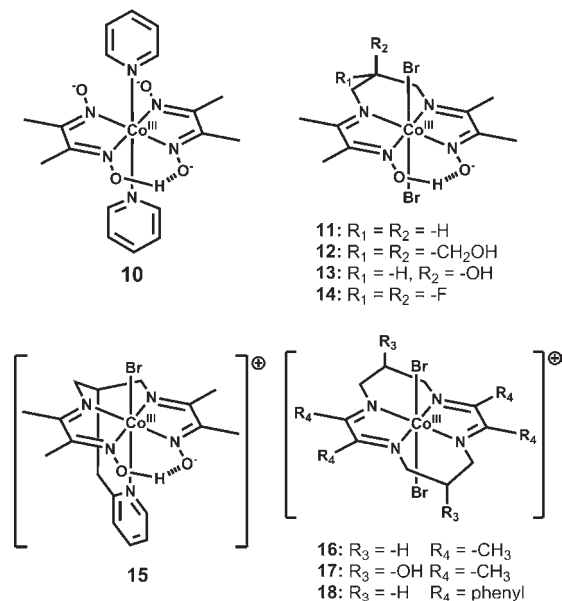


Figure 5. H₂ production for **1** with different WRCs. Conditions: 30 μM **1**, 500 μM Co, 1 M TEOA, 0.1 M HBF₄, H₂O, 10 mL, 380 nm, $q_{\text{h,p}} = 1.75 \times 10^{-7}$ einstein/s.

Scheme 2. Schematic Drawings of Water Reduction Catalysts **10–18**



presence of O₂, **1** remained completely stable. In CV experiments in H₂O, the reduction of **1** is irreversible (0.01–5 V/s). This indicated that reduced **1**⁻ is unstable in water and undergoes ligand loss on the upper microsecond to millisecond time scale. Since electron transfer to cobalt occurs within 1 μs , however, this decomposition does not limit catalytic performance of the studied systems in water.

pH Dependence. The pH dependencies of initial H₂ production and final TON_{Co} are shown in Figure 6 and Figures SI 6 and SI 7 (Supporting Information) for **10**, **11**, and **15**. The initial H₂ formation rates for all three WRCs decreased rapidly when going to more acidic solutions. Since the pK_a of [HTEOA]⁺ is 7.8,⁴² the concentration of free TEOA to reductively quench ***1** becomes small, and the reaction slows at lower pH. On the other hand, catalytic performance was better at lower pH, and the TON_{Co} reached a maximum at around pH 8. The pK_a of **10** in H₂O is 7.3

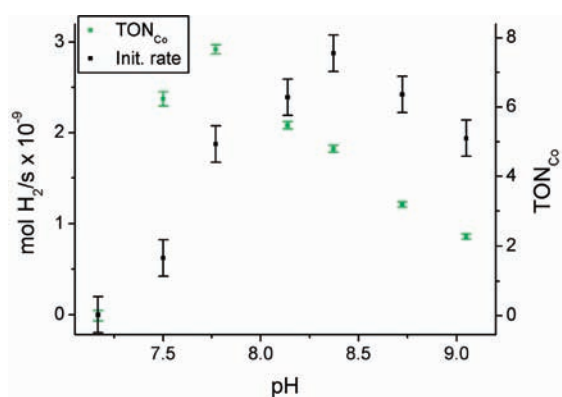


Figure 6. Initial H₂ production rates (left scale, ■, mol/s) and end TON_{Co} (right scale, green ■, H₂/Co) as a function of pH. Conditions: 30 μM **1**, 500 μM **10**, 1 M TEOA, varying HBF₄, H₂O, 10 mL, 380 nm, $q_{n,p} = 1.75 \times 10^{-7}$ einstein/s.

(but will be different for the corresponding Co^{II}, Co^I, and Co^{III}–H species), suggesting that most WRCs in these experiments are actually deprotonated on one oxime moiety. At higher pH values, both TOF and TON decrease. We observed a red shift in absorption at pH 10.5 in an irradiation experiment with **10**, indicative of a Co^I species accumulating in solution (see Figure SI 3, Supporting Information). Possibly, at high pH, protonation of Co^I becomes limiting, thus explaining the decrease in TOF. The accumulation of Co^I goes along with PS[−] accumulation, leading to the decomposition of PS (see Long-Term Performance section), and explains the decrease in TON at high pH.

Mechanism of Hydrogen Release. While in organic solvents, the nature of the hydrogen release step from Co^{III}–H for cobaloximes is believed to be homolytic,^{9,17,19,20} heterolytic and homolytic routes might be at work in parallel in protic media, depending on [Co] and pH.⁴³ In a similar system in DMF, at low [Co]_{tot}, a square dependence of H₂/s on [Co]_{tot} was found, indicative of a homolytic H₂ release step from Co^{III}–H, whereas at higher [Co]_{tot}, H₂/s was essentially limited by photon flux.^{9,19} In H₂O, if [**10**] was varied between 0.1 and 1 mM, no such dependence was found, indicating that the reaction is limited by photon flux (Figure SI 1, Supporting Information). The color change observed with **10** during irradiation (Figure SI 2, Supporting Information) strongly suggested an initial build up of Co^{II} ($\lambda_{\max} = 463$ nm, Figure SI 5, Supporting Information)^{18,44} which then remained the predominant component during catalysis. Over time, its absorption bleached, indicating decomposition. All other species such as Co^{III}, Co^I, or Co^{III}–H seem to be too short-lived to be detected. When the pH was increased to 10.5 (Figure SI 3, Supporting Information), new absorption bands at 625 and 550 nm appeared, characteristic for Co^I,^{17,18,20} as shown by comparison with an electrochemical reduction of a derivative of **10** in aprotic media (Figure SI 5, Supporting Information, $pK_a(\text{Co}^I) \approx 11-13$).^{16,45,46} Therefore, TONs are substantially reduced at high pH because Co^I and, subsequently, also PS[−] accumulate in solution (see Figure 6). On the other hand, this indicated that protonation of Co^I was not rate-limiting at low pH, but rather a follow-up reaction was. In the case of the DOH complexes, accumulation of Co^I occurred even at a pH of 8.7 (see Figure SI 5, Supporting Information), indicating that the respective $pK_a(\text{Co}^I)$ is lowered as compared to **10**. This could also suggest an alternative pathway to H₂ for the DOH complexes as compared to **10**, proceeding through the

Co^{II}–H intermediate.⁴⁷ Accordingly, the induction period observed before H₂ production, which has been shown to be related to the accumulation of reduction equivalents on the cobalt WRC,^{6,15} increases in the order dmGH < DOH < TIM. The exact set of reactions leading to H₂ release in H₂O solvent (e.g., if it occurs directly from Co^{III}–H or from Co^{II}–H, and if it occurs by a homolytic or heterolytic route)²⁰ still waits to be unraveled. As to be expected, experiments in D₂O, using 30 μM **1**, 500 μM WRC (**10**, **11**, or **15**), 1 M TEOA, 0.1 M HBF₄, and D₂O (~95%) produced D₂, thereby showing that the source of protons is the solvent indeed (see Figure SI 8 and Table SI 1, Supporting Information).

CONCLUSION

In conclusion, we present the first Re/Co based, light driven reductive half reaction to H₂ in H₂O. The catalytic cycle was investigated by time-resolved infrared spectroscopy. Upon excitation of the PS, reductive quenching by TEOA takes place ($k_q = 5-8 \times 10^7 \text{ M}^{-1} \text{ s}^{-1}$; $\Phi_{\text{cage}} = 0.75$), provided that the complexes are long-lived enough. It is followed by electron transfer from PS[−] to Co^{III} on the lower microsecond time range under our experimental conditions ($k_{\text{Co}^{\text{III}}} = 1.1 \times 10^9 \text{ M}^{-1} \text{ s}^{-1}$). This fast electron transfer is essential, given the instability of PS[−] on the millisecond time scale. Thus, under our conditions, the mechanism in the rhenium PS is almost identical to the one found in DMF.^{9,19} The only difference is the fact that no transfer of a second electron from oxidized TEOA was observed on a time scale up to 20 μs. We showed that, considering long-term performance, not the PS cycle, but the WRC cycle limits catalysis, as indicated by the correlation of TON_{Co} to the respective tetraene ligand framework. Thus, a decrease of catalytic performance in H₂O with respect to organic solvents is most likely due to a faster deactivation of the WRC catalyst, possibly by reduction of the tetraene moiety, as shown before. Understanding this deactivation in detail and increasing the rate of H₂ release with respect to the rate of deactivation, is thus the key to the development of long-term stable catalysts in H₂O.

The highest TON_{Re} was 550, while TON_{Co} did not exceed 17. Although TON_{Co}'s are low, our study is a proof of principle for the feasibility of H₂ formation from pure water with a Re/Co system. It serves as a base for further development of PSs and WRCs in particular. Our kinetic studies clearly showed that the WRC needs to be improved to achieve systems competitive with those in organic solvents. A pronounced pH dependence indicates that WRC deactivation is favored under basic conditions, whereas hydrogen elimination is favored under acidic conditions. The deactivation process decreases the hydrogen yield per WRC in water by about 2 orders of magnitude as compared to DMF as a solvent. We emphasize that kinetic, mechanistic, and thermodynamic studies are better defined in water than in organic solvents and will facilitate spectroscopic investigations and WRC design.

EXPERIMENTAL SECTION

All chemicals were of reagent grade and used without further purification. 1,3-Diaminopropane, 1,3-diamino-2-propanol, 2,2-bis(bromomethyl)-1,3-propanediol, picolyl chloride, diethyl malonate, benzil, and 2,3-butandione were purchased from Aldrich; diethyl difluoromalonate and 2,3-butane monoxime from Alfa Aesar; and CoBr₂·xH₂O, 54% aqueous HBF₄, and silver trifluoromethanesulfonate (AgTf₃SO) were purchased from Acros. Spectroscopy grade triethanolamine (TEOA), technical grade methyl-*tert*-butyl-ether (MTBE; distilled before use), [Co(ac)₂(OH₂)₄], pyridine

(py), benzylisocyanide (CNBz), 4-dimethylaminopyridine (4-Me₂Npy), dimethylglyoxime (dmgH₂), 2,2'-bipyridine (bipy), and phenanthroline (phen) were purchased from Fluka. Water was doubly distilled before use. Synthetic reactions were carried out under N₂ or Ar using standard Schlenk techniques. The syntheses of [Re(OH₂)(CO)₃bipy](TfIsO) (4),⁴⁸ [ReBr(CO)₃phen],⁴⁸ [Co(DOHpyr)Br](PF₆) (15),⁴⁹ [Co(TIM^{Me})Br₂] (16),⁵⁰ and [Co(TIM^{Ph})Br₂] (18)⁵¹ as well as the ligand fragment 2,2-bis(aminomethyl)propane-1,3-diol⁵² have been described in the literature.

SYNTHESES

[Re(py)(CO)₃bipy](TfIsO) (1). Complex 4 (296.5 mg, 0.5 mmol) was dissolved in 25 mL of MeOH, and pyridine (100 μL, 1.29 mmol) was added. The resulting solution was refluxed for 12 h, evaporated to dryness, suspended in 25 mL of MTBE, filtered, washed with MTBE, and dried in vacuo. Yield: 320.5 mg (98%) of an off-yellow powder. λ_{max}(H₂O): 343 nm (ε = 3650 M⁻¹ cm⁻¹). λ_{em}(H₂O): 567 nm (Φ_{em} = 0.0098 ± 0.0003). IR (KBr): 2026 (s), 1923 (s), 1907 (s), 1280 (m), 1260 (m), 1030 (m), 637 (m). ¹H NMR (200 MHz, d⁶-dmsO, ppm): 9.32 (d, 2 H), 8.70 (d, 2 H), 8.40 (m, 4 H), 7.92 (m, 3 H), 7.43 (t, 2 H). ESI-MS(MeOH): *m/z* 506.0 [M - TfIsO]⁺ (100%), 426.9 [M - TfIsO-pyridine]⁺ (2%). HPLC: 15.08 min. Anal. Calcd. for C₁₉H₁₃F₃N₃O₆ReS (%): C, 34.86; H, 2.00; N, 6.42. Found: C, 34.66; H, 1.99; N, 6.62.

[Re(CNBz)(CO)₃bipy](TfIsO) (2). Complex 4 (29.7 mg, 50 μmol) was dissolved in 5 mL of MeOH and benzylisocyanide (61 μL, 0.5 mmol) was added. The resulting solution was stirred for 36 h, evaporated to dryness, suspended in 5 mL of MTBE, filtered, washed with MTBE, and dried in vacuo. Yield: 33.5 mg (97%) of an off-yellow powder. λ_{max}(H₂O): 337 nm (sh; ε = 3800 M⁻¹ cm⁻¹). λ_{em}(H₂O): 527 nm (Φ_{em} = 0.087 ± 0.003). IR (KBr): 2223 (s), 2041 (s), 1956 (s), 1935 (s), 1281 (m), 1258 (m), 1030 (m), 773 (m). ¹H NMR (200 MHz, d⁶-dmsO, ppm): 9.08 (d, 2 H), 8.81 (d, 2 H), 8.41 (t, 2 H), 7.82 (t, 2 H), 7.27 (m, 3 H), 6.89 (m, 2 H), 5.01 (s, 2 H). ESI-MS(MeOH): *m/z* 544.1 [M - TfIsO]⁺ (100%). HPLC: 15.79 min. Anal. Calcd. for C₂₂H₁₅F₃N₃O₆ReS (%): C, 38.15; H, 2.18; N, 6.07. Found: C, 38.14; H, 2.21; N, 6.04.

[Re(4-Me₂Npy)(CO)₃bipy](TfIsO) (3). Complex 4 (30.5 mg, 51 μmol) was dissolved in 5 mL of MeOH, and 4-dimethylaminopyridine (20.5 mg, 0.17 mmol) was added. The resulting orange solution was refluxed for 4 h, evaporated to dryness, suspended in 5 mL of MTBE, filtered, washed with MTBE, and dried in vacuo. Yield: 31.4 mg (90%) of a yellow powder. λ_{max}(H₂O): 368 nm (ε = 2450 M⁻¹ cm⁻¹). λ_{em}(H₂O): 602 nm (Φ_{em} = 0.00029 ± 0.00001). IR (KBr): 2029 (s), 1935 (s), 1903 (s), 1627 (m), 1275 (m), 1230 (m), 1025 (m), 637 (m). ¹H NMR (300 MHz, d⁶-dmsO, ppm): 9.29 (d, 2 H), 8.73 (d, 2 H), 8.41 (t, 2 H), 7.90 (t, 2 H), 7.65 (d, 2 H), 6.47 (d, 2 H), 2.90 (s, 6 H). ESI-MS(MeOH): *m/z* 549.1 [M - TfIsO]⁺ (100%). HPLC: 15.78 min. Anal. Calcd. for C₂₁H₁₈F₃N₄O₆ReS (%): C, 36.15; H, 2.60; N, 8.03. Found: C, 36.01; H, 2.67; N, 8.29.

[Re(OH₂)(CO)₃phen](TfIsO) (8). [ReBr(CO)₃phen] (529.9 mg, 1 mmol) was suspended in 80 mL of MeOH, and AgTfIsO (256.5 mg, 1 mmol), dissolved in 10 mL of MeOH, was added. The suspension was, under exclusion of light, stirred overnight and sonicated several times to avoid the formation of large colloidal particles. AgBr was removed quantitatively by filtration and the resulting, clear orange solution evaporated to dryness. The residue was then refluxed for 2 h in 200 mL of H₂O, filtered to remove any insoluble material, and the resulting yellow

solution lyophilized. Yield: 673.0 mg (109%) of an orange powder. λ_{max}(H₂O): 360 nm (sh, ε = 3400 M⁻¹ cm⁻¹). λ_{em}(H₂O): 578 nm (Φ_{em} = 0.00099 ± 0.00002). IR (KBr): 2035 (s), 1919 (s), 1735 (m), 1618 (m), 1266 (m), 1231 (m), 1031 (m), 638 (m). ¹H NMR (300 MHz, d⁶-dmsO, ppm): 9.52 (dd, 2 H), 9.06 (d, 2 H), 8.37 (s, 2 H), 8.19 (dd, 2 H), 7.50 (s, 2 H). ESI-MS(MeOH): *m/z* 468.8 [M - TfIsO]⁺ (25%), 450.9 [M - TfIsO-OH₂]⁺ (100%). HPLC: 15.29 min. Anal. Calcd. for C₁₆H₁₀F₃N₂O₇ReS (%): C, 31.12; H, 1.63; N, 4.54. Found: C, 30.98; H, 1.79; N, 4.31.

[Re(py)(CO)₃phen](TfIsO) (5). Complex 8 (30.4 mg, 50 μmol) was dissolved in 5 mL of pyridine, and the resulting solution was stirred for 10 days, evaporated to dryness, suspended in 5 mL of MTBE, filtered, washed with MTBE, and dried in vacuo. Yield: 26.0 mg (77%) of an off-yellow powder. λ_{max}(H₂O): 362 nm (ε = 3350 M⁻¹ cm⁻¹). λ_{em}(H₂O): 550 nm (Φ_{em} = 0.039 ± 0.001). IR (KBr): 2030 (s), 1918 (s), 1263 (m), 1028 (m), 637 (m). ¹H NMR (300 MHz, d⁶-dmsO, ppm): 9.77 (d, 2 H), 9.04 (d, 2 H), 8.46 (d, 2 H), 8.31 (s, 2 H), 8.26 (dd, 2 H), 7.86 (t, 1 H), 7.32 (t, 2 H). ESI-MS(MeOH): *m/z* 530.0 [M - TfIsO]⁺ (100%), 451.0 [M - TfIsO-pyridine]⁺ (10%). HPLC: 15.30 min. Anal. Calcd. for C₂₁H₁₃F₃N₃O₆ReS (%): C, 37.17; H, 1.93; N, 6.19. Found: C, 37.23; H, 1.97; N, 6.39.

[Re(CNBz)(CO)₃phen](TfIsO) (6). Complex 8 (30.7 mg, 50 μmol) was dissolved in 5 mL of MeOH, and benzylisocyanide (20 μL, 0.17 mmol) was added. The resulting solution was stirred for 10 days, evaporated to dryness, suspended in 5 mL of MTBE by sonication, filtered, washed with MTBE, and dried in vacuo. Yield: 30.5 mg (85%) of an off-yellow powder. λ_{max}(H₂O): 360 nm (sh; ε = 2600 M⁻¹ cm⁻¹). λ_{em}(H₂O): 515 nm (Φ_{em} = 0.208 ± 0.004). IR (KBr): 2201 (m), 2044 (s), 1966 (s), 1938 (s), 1267 (m), 1031 (m), 637 (m). ¹H NMR (300 MHz, d⁶-dmsO, ppm): 9.51 (d, 2 H), 9.03 (d, 2 H), 8.39 (s, 2 H), 8.16 (dd, 2 H), 7.22 (t, 1 H), 7.10 (t, 2 H), 8.62 (d, 2 H), 4.87 (s, 2 H). ESI-MS(THF): *m/z* 568.0 [M - TfIsO]⁺ (100%). HPLC: 15.79 min. Anal. Calcd. for C₂₄H₁₅F₃N₃O₆ReS (%): C, 40.22; H, 2.11; N, 5.86. Found: C, 40.32; H, 2.09; N, 5.95.

[Re(4-Me₂Npy)(CO)₃phen](TfIsO) (7). Complex 8 (30.5 mg, 50 μmol) was dissolved in 20 mL of MeOH, and 4-dimethylaminopyridine (22 mg, 0.18 mmol) was added. The resulting orange solution was refluxed for 100 h, evaporated close to dryness, suspended in 5 mL of MTBE, filtered, washed with MTBE, and dried in vacuo. Yield: 23.6 mg (65%) of a yellow powder. λ_{max}(H₂O): 368 nm (ε = 3000 M⁻¹ cm⁻¹). λ_{em}(H₂O): 592 nm (Φ_{em} = 0.0011 ± 0.0001). IR (KBr): 2024 (s), 1936 (s), 1921 (s), 1628 (m), 1270 (m), 1032 (m), 637 (m). ¹H NMR (300 MHz, d⁶-dmsO, ppm): 9.74 (d, 2 H), 9.04 (d, 2 H), 8.33 (s, 2 H), 8.24 (dd, 2 H), 7.71 (d, 2 H), 6.35 (d, 2 H), 2.82 (s, 6 H). ESI-MS(MeOH): *m/z* 573.2 [M - TfIsO]⁺ (100%). HPLC: 16.04 min. Anal. Calcd. for C₂₃H₁₈F₃N₄O₆ReS (%): C, 38.28; H, 2.51; N, 7.76. Found: C, 37.94; H, 2.38; N, 7.46.

[Co(py)₂(dmgH)(dmg)] (10). To [Co(ac)₂(OH₂)₄] (622.5 mg, 2.5 mmol) in 10 mL of MeOH was added 2 mL of pyridine (24.8 mmol) under stirring. The dark violet solution was degassed and flushed with argon several times before dmgH₂ (581 mg, 5 mmol) was added as a solid. Immediate formation of a brown precipitate occurs. After 5 min of stirring under an argon atmosphere, air was gently bubbled through the suspension for 1 h and the solvent removed in vacuo. The residue was then taken up in 50 mL H₂O and filtered to remove any insoluble material. Slow addition of 1 M NaOH (5 mL, 2 equivalents) resulted in the formation of brownish, cubic crystals. Filtration and washing with

cold H₂O afforded 843.4 mg (1.89 mmol, 76%) **10**. IR (KBr): 1291 (s), 772 (s), 698 (s), 515 (s). ¹H NMR (200 MHz, D₂O, ppm): 8.30 (d, 4 H), 7.76 (t, 2 H), 7.26 (t, 4 H), 2.13 (s, 6 H), 1.92 (s, 6 H). ESI-MS(MeOH): *m/z* = 447.1 [MH]⁺ (35%), 289.3 [MH - 2 pyridine]⁺ (100%). HPLC: 13.69 min. Anal. Calcd. for C₁₈H₂₃CoN₆O₄ (%): C, 48.44; H, 5.19; N, 18.83. Found: C, 48.31; H, 5.18; N, 18.34.

2,2-Difluoro-1,3-diaminopropane. Diethyl difluoromalonate (1.7 g, 8.71 mmol) was dissolved in a solution of ammonia in methanol (saturated at 0 °C). After 2 days, the solvent was removed, and the residue was dissolved in 8 mL of dry THF. To the resulting suspension (kept at 0 °C) was added cautiously over 20 min 80 mL of a 1 M solution of BH₃·THF. Once the addition was complete, the mixture was refluxed for 4 h. After cooling to 0 °C, 7 mL of H₂O was added very carefully to destroy excess diborane. The solution was evaporated to dryness, and the residue was slowly treated with 35 mL of 6 N HCl. After refluxing for another 4 h, the solution was left to stand overnight. The precipitate was filtered off, and the solvent was removed. The addition of 17 mL of H₂O and 12 mL of 6 N NaOH and extraction with CH₂Cl₂ yielded 872 mg (7.9 mmol, 91%) of 2,2-difluoro-1,3-diaminopropane as a colorless oil. ¹H NMR (200 MHz, DMSO, ppm): 2.88 (t, 4 H).

General Procedure for CoDOH-type complexes. After stirring a solution of the corresponding diamine (0.4 M) and 2,3-butanedione monoxime (0.8 M) in EtOH for seven days, the solution was degassed and combined with a degassed solution of CoBr₂·*x*H₂O (2 eq, 0.8 M) in EtOH. Air was bubbled through the reaction for 10 min, and the solution was then left to stand several days for crystallization. Filtration and washing with cold water afforded a green, crystalline product with typical yields between 5 and 25%.

[CoDOHBr₂] (**11**). IR (KBr): 1521 (m), 1136 (m). ¹H NMR (200 MHz, Acetone, ppm): 19.58 (s, NOH, 1 H), 4.14 (m, CH₂, 6 H), 2.68 (s, CH₃, 6 H), 2.52 (s, CH₃, 6 H). ESI-MS(MeOH): *m/z* 480.8 [M + Na]⁺ (100%). Anal. Calcd. for C₁₁H₁₉Br₂CoN₄O₂ (%): C, 28.84; H, 4.18; N, 12.23. Found: C, 29.05; H, 4.21; N, 12.30.

[Co(DOH(COH)₂)Br₂] (**12**). IR (KBr): 1509 (m), 1041 (m). ¹H NMR (200 MHz, DMSO, ppm): 19.07 (s, NOH, 1 H), 4.75 (t, OH, 2 H), 4.02 (s, NCH₂, 4 H), 3.70 (d, OCH₂, 4 H), 2.64 (s, CH₃, 6 H), 2.51 (s, CH₃, 6 H). ESI-MS(MeOH): *m/z* 427 [M - Br]⁺ (100%). Anal. Calcd. for C₁₃H₂₃Br₂CoN₄O₄ (%): C, 30.14; H, 4.47; N, 10.81. Found: C, 29.97; H, 4.57; N, 10.80.

[CoDOHOHBr₂] (**13**). IR (KBr): 1513 (m), 1146 (m). ¹H NMR (200 MHz, DMSO, ppm): 19.29 (s, NOH, 1 H), 5.69 (d, OH, 1 H), 4.54 (m, CH, 1 H), 4.32 (d, HCH, 2 H), 3.70 (dd, HCH, 2 H), 2.66 (s, CH₃, 6 H). ESI-MS(MeOH): *m/z* 314 [M - 2Br]⁺ (100%). Anal. Calcd. for C₁₁H₁₉Br₂CoN₄O₃ (%): C, 27.87; H, 4.04; N, 11.82. Found: C, 27.76; H, 3.88; N, 12.04.

[CoDOHF₂Br₂] (**14**). IR (KBr): 1499 (m), 1302 (m), 1134 (m), 1093 (m). ¹H NMR (200 MHz, DMSO, ppm): 19.12 (s, NOH, 1 H), 4.59 (t, CH₂, 4 H), 2.71 (s, CH₃, 6 H). ESI-MS(MeOH): *m/z* 343 [M - 2Br]⁺ (100%). Anal. Calcd. for C₁₁H₁₇Br₂CoF₂N₄O₂ (%): C, 26.74; H, 3.47; N, 11.34. Found: C, 26.72; H, 3.39; N, 11.38.

[Co(TIMOH)Br₂]Br (**17**). Compound **17** was synthesized according to the literature procedure for **16**.⁵⁰ IR (KBr): 1420 (m), 1215 (m), 1098 (m). ¹H NMR (200 MHz, Acetone, ppm): 5.95 and 5.82 (2 s, CH, 2 H), 4.62 (s, OH, 2 H), 4.37 (d, HCH, 4 H), 3.76 (t, HCH, 4 H), 2.52 (s, CH₃, 12 H). ESI-MS(MeOH): *m/z* 499 [M]⁺ (100%). Anal. Calcd. for C₁₄H₂₄Br₂CoF₂N₄O₂

(%): C, 29.04; H, 4.17; N, 9.68. Found: C, 29.05; H, 4.16; N, 9.64.

SPECTROSCOPY

Mass spectra were measured on a Bruker Esquire HCT (ESI) instrument, and only characteristic fragments are given. The solvent flow rate for ESI measurements was 5 μL min⁻¹; a nebulizer pressure of 15 psi and a dry gas flow rate of 5 L min⁻¹ at a dry gas temperature of 300 °C were used.

Elemental analyses were performed on a LecoCHNS-932 elemental analyzer.

¹H NMR spectra were recorded on Varian Mercury and Varian Gemini-2000 spectrometers (¹H at 199.97 and 300.08 MHz, respectively). The chemical shifts are reported relative to residual solvent protons as a reference.

UV-vis spectra were measured using a Cary 50 spectrometer with solution samples in 1 cm quartz cells. If necessary, cells with silicon septa lids were used to keep samples under an inert gas atmosphere during measurements.

IR spectra were recorded on a Bio PerkinElmer Spectrum-BXFT-IR spectrometer with samples in compressed KBr pellets.

Electrochemical measurements were carried out in DMF containing 0.1 M [TBA][PF₆] as a conducting electrolyte. A Metrohm 757VA Computrace electrochemical analyzer was used with a standard three-electrode setup of glassy carbon working (i.d. = 3 mm) and Pt auxiliary electrodes and a Ag/AgCl reference electrode. All potentials are given vs Ag/AgCl and are referenced with Fc/Fc⁺ at +500 mV. Spectroelectrochemical analysis was performed in an optical transparent thin layer electrolysis (OTTLE) cell^{53,54} in the UV-vis spectrometer described above. The working electrode was a platinum mesh immersed into the OTTLE cell. The auxiliary electrode was a platinum wire in a compartment separated by a diaphragm, and the reference electrode was a Ag/AgCl electrode.

HPLC measurements were performed on a VWR LaChrome Elite using a Nucleodur C18 Gravity column operated in an oven (L-2350) at 40 °C and using a PDA detector (L-2450). The gradient was as follows: A = 0.1% TFA, 10% MeOH, H₂O; D = MeOH; flow rate = 0.5 mL/min; 0–5 min 100% A; 5–15 min 0–100% D; 15–18 min 100% D. Control runs before and after catalysis were systematically performed using 10 μL of the reaction solution in DMF. Under these conditions, dmHg₂ gave a broad peak at 6.4 min and **I** a defined peak at 17.04 min.

Luminescence measurements were performed on a Perkin-Elmer LSS0B fluorescence spectrometer with argon-purged solution samples in 1 cm cells. Luminescence lifetime measurements were performed on an Edinburgh Instrument F900 equipped with an nF900 ns flash lamp filled with hydrogen (operating at 0.4 bar and frequency 40 kHz). Luminescence quantum yields were determined relative to coumarin **I** in ethanol (0.64)⁵⁵ according to a literature procedure.⁵⁶

Gas chromatograms were recorded using a Varian CP-3800 gas chromatograph with argon as the carrier gas and a 3 m × 2 mm packed molecular sieve 13X 80–100 column. The gas flow was set to 20 mL/min. The oven was operated isothermally at 100 °C. An argon flow of usually 10.8 mL/min (adjusted with a manual flow controller (Porter, 100) and referenced with a flow meter (MS Wil GmbH)) was passed through the reaction mixture and into the GC, where 100 μL gas samples were automatically injected in defined time intervals (usually 5 min) using a 6-Port-2-Position Valve from Vicci. The gases were

detected using a thermal conductivity detector (Varian) operated at 150 °C (retention times are 1.22 and 1.29 min for H₂ and D₂, respectively). Hydrogen or deuterium production rates were calibrated by introducing a known flow of the pure gas by a Single Syringe Pump (70–2208 from Harvard Apparatus, using a 2.5 mL Hamilton GASTIGHT #1002 syringe and a Teflon tube) to the 60 mL Schlenk reactor containing 1 M TEOA in DMF. Plotting of the peak area for hydrogen with respect to deuterium versus the flow rates used gave linear fits. The slope of these fits depended linearly on the argon flow through the solution. Varying the argon flow thus allowed detection of smaller hydrogen/deuterium production rates, although at a higher response time (20 min for 10.8 mL/min). This setup allowed us to detect H₂/s $\geq 0.3 \times 10^{-9}$ mol s⁻¹ (standard deviation is $\leq 0.2 \times 10^{-9}$ mol s⁻¹) with respect to D₂/s $\geq 0.2 \times 10^{-9}$ mol s⁻¹ (standard deviation is $\sim 0.1 \times 10^{-9}$ mol s⁻¹).

Photochemical measurements were carried out in a 60 mL septum capped Schlenk reactor containing a Teflon stirrer at 500 rpm. A total of 10 mL of a solution containing the respective mixture in H₂O was prepared, wrapped in black foil, and degassed using an argon-purged Schlenk line. The mixture was equilibrated under 1.5 bar of argon pressure for 15 min and then transferred to a dark room for illumination. The light source was a 380 nm high flux LED from Rhopoint Components LTD (OTLH-0280-UV; CPC reflector for Shark LED; irradiated directly from below; current control at usually 200 mA; $q_{n,p} = 1.75 \times 10^{-7}$ einstein/s). If necessary, the radiant flux was varied by adjustment of the current through the LED. The radiant flux at different currents was calibrated using actinometry. A constant flow of usually 10.8 mL/min of argon was passed through the solution and into a six-port valve at the GC, where 100 μ L gas samples were injected into the GC-TCD gas analyzer in defined intervals. Integration of the production rate versus time gave the total amount of hydrogen produced. Quantum yields were measured in a 1 \times 1 cm, 3.5 mL quartz cell from Helma, equipped with a septa cap for gas sampling during photolysis. The degassed solution was stirred and irradiated with a 380 nm high flux LED from Rhopoint Components LTD (OTLH-0280-UV), projected onto the cell ($q_{n,p} = 4.8 \times 10^{-9}$ einstein/s). A total of 92% of these photons are absorbed by a 0.5 mM solution of **1** ($\epsilon_{380\text{ nm}} = 2150\text{ cm}^{-1}\text{ M}^{-1}$). Quantum yields are given as H per absorbed photon.

UV–Pump–IR–Probe Spectroscopy. The system for UV–pump–IR–probe spectroscopy consists of two synchronized³¹ Ti:sapphire-oscillator/regenerative amplifier femtosecond laser systems operating at 800 nm (Spectra Physics, pulse duration ~ 100 fs, repetition rate 1 kHz, energy $\sim 600\ \mu\text{J}$ /pulse), allowing us to cover the time range from 2 ps to 20 μs . Laser system 1 was frequency-doubled with a BBO crystal. The obtained 400 nm pulses ($\sim 1.3\ \mu\text{J}$ /pulse) were subsequently focused into the sample cell (100- μm -thick) with a spot size of $\sim 200\ \mu\text{m}$ in diameter. Laser system 2 pumped a white light seeded two-stage BBO optical parametric amplifier (OPA),⁵⁷ the signal and idler pulses of which were difference frequency mixed in a AgGaS₂ crystal. They were separated into two parts to achieve broadband probe and reference pulses. These IR–probe pulses were focused into the sample cell, the probe pulse in spatial overlap with the 400 nm pump pulse, while polarization of the pump and probe pulses were set to a relative angle of 54.7° to allow for direct measurement of the anisotropy free magic angle signal. Reference and probe pulses were dispersed in a monochromator (SPEX Triax Series) and imaged onto a 2 \times 64 pixel MCT

(Mercury Cadmium Telluride) detector array (InfraRed Associates Inc.), resulting in a spectral resolution of 3.5 cm⁻¹. To ensure efficient exchange of the excited volume, the sample was pumped rapidly by a peristaltic pump (Ismatec BVP equipped with EasyLoad II pump-head) to a small sealed reservoir ($V \approx 3$ mL). The pressurized flow of the reservoir transferred the sample through the flow cell and finally back to the sample tank, which was protected from light. Since TEOA is an aggressive compound, the pump-head was equipped with chemically resistant fluoroelastomer tubing from Gore (Chem-Sure). To exclude any oxygen, the sample solution was purged with argon for at least 60 min before and during measurements. During the course of a measurement, sample degradation remained negligibly small (<5%), which was checked via HPLC analysis before and afterward.

■ ASSOCIATED CONTENT

S Supporting Information. H₂ production as a function of [Co] and pH, absorption changes during catalysis, spectroelectrochemistry, and CV of [Co(py)₂(dmgH)₂]PF₆ are available free of charge via the Internet at <http://pubs.acs.org>.

W Web Enhanced Feature. An animated image of a related experiment is available.

■ AUTHOR INFORMATION

Corresponding Author

*E-mail: ariel@aci.uzh.ch.

Present Addresses

⁵Current address: Department of Environment, Energy and Mobility, EMPA, Überlandstrasse 129, CH-8600 Dübendorf, Switzerland

■ ACKNOWLEDGMENT

We acknowledge the Swiss National Science Foundation (SNF grant No. 200021-119798) and the Kanton Zürich for financial support.

■ REFERENCES

- (1) Nicola Armaroli, V. B. *Angew. Chem.* **2007**, *119*, 52–67.
- (2) Krishnan, C. V.; Creutz, C.; Mahajan, D.; Schwarz, H. A.; Sutin, N. *Isr. J. Chem.* **1982**, *22*, 98–106.
- (3) Cline, E. D.; Adamson, S. E.; Bernhard, S. *Inorg. Chem.* **2008**, *47*, 10378–10388.
- (4) Krishnan, C. V.; Brunschwigg, B. S.; Creutz, C.; Sutin, N. *J. Am. Chem. Soc.* **1985**, *107*, 2005–2015.
- (5) Lazarides, T.; McCormick, T.; Du, P. W.; Luo, G. G.; Lindley, B.; Eisenberg, R. *J. Am. Chem. Soc.* **2009**, *131*, 9192–9194.
- (6) Du, P.; Schneider, J.; Luo, G.; Brennessel, W. W.; Eisenberg, R. *Inorg. Chem.* **2009**, *48*, 4952–4962.
- (7) Fihri, A.; Artero, V.; Razavet, M.; Baffert, C.; Leibl, W.; Fontecave, M. *Angew. Chem., Int. Ed.* **2008**, *47*, 564–567.
- (8) Hawecker, J.; Lehn, J. M.; Ziessel, R. *New J. Chem.* **1983**, *7*, 271–277.
- (9) Probst, B.; Kolano, C.; Hamm, P.; Alberto, R. *Inorg. Chem.* **2009**, *48*, 1836–1843.
- (10) Li, C.; Wang, M.; Pan, J.; Zhang, P.; Zhang, R.; Sun, L. *J. Organomet. Chem.* **2009**, *694*, 2814–2819.
- (11) Kalyanasundaram, K.; Kiwi, J.; Gratzel, M. *Helv. Chim. Acta* **1978**, *61*, 2720–2730.

- (12) Moradpour, A.; Amouyal, E.; Keller, P.; Kagan, H. *Nouv. J. Chim.* **1978**, *2*, 547–549.
- (13) Lehn, J. M.; Sauvage, J. P. *Nouv. J. Chim.* **1977**, *1*, 449–451.
- (14) Pac, C.; Ishii, K.; Yanagida, S. *Chem. Lett.* **1989**, 765–768.
- (15) McCormick, T. M.; Calitree, B. D.; Orchard, A.; Kraut, N. D.; Bright, F. V.; Detty, M. R.; Eisenberg, R. *J. Am. Chem. Soc.* **2010**, *132*, 15480–15483.
- (16) Kellett, R. M.; Spiro, T. G. *Inorg. Chem.* **1985**, *24*, 2373–2377.
- (17) Hu, X.; Brunschwig, B. S.; Peters, J. C. *J. Am. Chem. Soc.* **2007**, *129*, 8988–8998.
- (18) Du, P. W.; Knowles, K.; Eisenberg, R. *J. Am. Chem. Soc.* **2008**, *130*, 12576–12577.
- (19) Probst, B.; Rodenberg, A.; Guttentag, M.; Hamm, P.; Alberto, R. *Inorg. Chem.* **2010**, *49*, 6453–6460.
- (20) Dempsey, J. L.; Winkler, J. R.; Gray, H. B. *J. Am. Chem. Soc.* **2010**, *132*, 1060–1065.
- (21) Krishnan, C. V.; Sutin, N. *J. Am. Chem. Soc.* **1981**, *103*, 2141–2142.
- (22) Hawecker, J.; Lehn, J. M.; Ziessel, R. *New J. Chem.* **1983**, *7*, 271–277.
- (23) Duan, L.; Xu, Y.; Zhang, P.; Wang, M.; Sun, L. *Inorg. Chem.* **2009**, *49*, 209–215.
- (24) Comte, P.; Nazeeruddin, M. K.; Rotzinger, F. P.; Frank, A. J.; Gratzel, M. *J. Mol. Catal.* **1989**, *52*, 63–84.
- (25) Geletii, Y. V.; Huang, Z.; Hou, Y.; Musaev, D. G.; Lian, T.; Hill, C. L. *J. Am. Chem. Soc.* **2009**, *131*, 7522–7523.
- (26) Yin, Q. S.; Tan, J. M.; Besson, C.; Geletii, Y. V.; Musaev, D. G.; Kuznetsov, A. E.; Luo, Z.; Hardcastle, K. I.; Hill, C. L. *Science* **2010**, *328*, 342–345.
- (27) Excited state lifetimes do correlate with the HOMO–LUMO gap of the complexes, as estimated from the emission wavelength respective to the electrochemical data given in Table 1.
- (28) Modification of the loop size (to 500 μL), reduction of Ar flow rate (5 mL/min), and reduction of the head space (2 mL), as compared to the setup described in the Experimental Section, provided sufficient sensitivity for H₂ measurements with **3**.
- (29) Experiments with **2**, **3**, **6**, and **7** were not possible due to solubility issues in the buffer system at concentrations needed for UV–pump–IR–probe measurements.
- (30) Classical Stern–Volmer plots of luminescence intensities vs [TEOA] are not possible in H₂O because intensity changes due to viscosity/polarity changes in the solvent upon addition of TEOA. Further, deaerated solutions of **1** and TEOA in H₂O are not photostable.
- (31) Bredenbeck, J.; Helbing, J.; Hamm, P. *Rev. Sci. Instrum.* **2004**, *75*, 4462–4466.
- (32) Busby, M.; Matousek, P.; Towrie, M.; Vlcek, A. *Inorg. Chim. Acta* **2007**, *360*, 885–896.
- (33) Vlcek, A.; Busby, M. *Coord. Chem. Rev.* **2006**, *250*, 1755–1762.
- (34) Rodriguez, A. M. B.; Gabriellson, A.; Motevalli, M.; Matousek, P.; Towrie, M.; Sebera, J.; Zalis, S.; Vlcek, A. *J. Phys. Chem. A* **2005**, *109*, 5016–5025.
- (35) Dattelbaum, D. M.; Omberg, K. M.; Hay, P. J.; Gebhart, N. L.; Martin, R. L.; Schoonover, J. R.; Meyer, T. J. *J. Phys. Chem. A* **2004**, *108*, 3527–3536.
- (36) George, M. W.; Johnson, F. P. A.; Westwell, J. R.; Hodges, P. M.; Turner, J. J. *J. Chem. Soc., Dalton Trans.* **1993**, 2977–2979.
- (37) Glyn, P.; George, M. W.; Hodges, P. M.; Turner, J. J. *J. Chem. Soc., Chem. Comm.* **1989**, 1655–1657.
- (38) Dattelbaum, D. M.; Omberg, K. M.; Schoonover, J. R.; Martin, R. L.; Meyer, T. J. *Inorg. Chem.* **2002**, *41*, 6071–6079.
- (39) Hayashi, Y.; Kita, S.; Brunschwig, B. S.; Fujita, E. *J. Am. Chem. Soc.* **2003**, *125*, 11976–11987.
- (40) Simandi, L. I.; Szeverenyi, Z.; Budozahonyi, E. *Inorg. Nuc. Chem. Lett.* **1975**, *11*, 773–777.
- (41) Hori, H.; Ishihara, J.; Koike, K.; Takeuchi, K.; Ibusuki, T.; Ishitani, O. *J. Photochem. Photobiol. A* **1999**, *120*, 119–124.
- (42) Izutsu, K. *Acid-base dissociation constants in dipolar aprotic solvents*; Blackwell Scientific Publications: Oxford, 1990; p 166.
- (43) Chao, T. H.; Espenson, J. H. *J. Am. Chem. Soc.* **1978**, *100*, 129–133.
- (44) Heckman, R. A.; Espenson, J. H. *Inorg. Chem.* **1979**, *18*, 38–43.
- (45) Schrauzer, G. N.; Holland, R. J. *J. Am. Chem. Soc.* **1971**, *93*, 1505–1506.
- (46) Baffert, C.; Artero, V.; Fontecave, M. *Inorg. Chem.* **2007**, *46*, 1817–1824.
- (47) Dempsey, J. L.; Brunschwig, B. S.; Winkler, J. R.; Gray, H. B. *Acc. Chem. Res.* **2009**, *42*, 1995–2004.
- (48) Kurz, P.; Probst, B.; Spingler, B.; Alberto, R. *Eur. J. Inorg. Chem.* **2006**, 2966–2974.
- (49) Gerli, A.; Sabat, M.; Marzilli, L. G. *J. Am. Chem. Soc.* **1992**, *114*, 6711–6718.
- (50) Jackels, S. C.; Busch, D. H.; Barefiel, E.; Rose, N. J.; Farmery, K. *Inorg. Chem.* **1972**, *11*, 2893–.
- (51) Welsh, W. A.; Reynolds, G. J.; Henry, P. M. *Inorg. Chem.* **1977**, *16*, 2558–2561.
- (52) Virta, P.; Leppanen, M.; Lonnberg, H. *J. Org. Chem.* **2004**, *69*, 2008–2016.
- (53) Brett, A. M. C. F. O. *Electroanalysis* **1992**, *4*, 911–914.
- (54) Deangelis, T. P.; Heineman, W. R. *J. Chem. Educ.* **1976**, *53*, 594–597.
- (55) Olmsted, J. *J. Phys. Chem.* **1979**, *83*, 2581–2584.
- (56) Williams, A. T. R.; Winfield, S. A.; Miller, J. N. *Analyst* **1983**, *108*, 1067–1071.
- (57) Hamm, P.; Kaindl, R. A.; Stenger, J. *Opt. Lett.* **2000**, *25*, 1798–1800.